Fermilab Library
0 1160 0033397

KEK-TH-387
KEK Preprint 93-205
February 1994
H

Gluon Distribution in the Photon*

Isamu WATANABE†

Theory Group, KEK
1-1 Oho, Tsukuba, Ibaraki 305, Japan

ABSTRACT

We study systematically the sensitivity of the photon structure function data on the gluon contents of the photon, by using the leading order Altarelli–Parisi (AP) equations. Charm quark contribution is studied in the quark parton model, the massive quark AP equations of Glück, Hoffmann and Reya, and in the massless four-flavor AP equations. The present photon structure function data are found to allow wide range of gluon distributions in the photon. We give a set of the scale-dependent parton distributions in the photon (WHIT1 to WHIT6), which have systematically different gluon contents. Sensitivity of the structure function at small x and that of the total charm quark production cross section to the effective gluon distribution are discussed.

* Invited talk presented at *"The Second Workshop on TRISTAN Physics at High Luminosities"*, KEK, Tsukuba, Japan, Nov. 24–26, 1993.

† Junior Scientist Fellow of the Japan Society for the Promotion of Science. Work supported in part by the Grant-in-Aid for Scientific Research from the Ministry of Education, Science and Culture of Japan.

APR 4 1994
LIBRARY

National Laboratory for High Energy Physics, 1994

KEK Reports are available from:

Technical Information & Library
National Laboratory for High Energy Physics
1-1 Oho, Tsukuba-shi
Ibaraki-ken, 305
JAPAN

Phone: 0298-64-1171
Telex: 3652-534 (Domestic)
(0)3652-534 (International)
Fax: 0298-64-4604
Cable: KEK OHO
E-mail: LIBRARY@JPNKEKVX (Bitnet Address)
library@kekvax.kek.jp (Internet Address)

1 Introduction

The deep structure of the photon has been expected to be calculable perturbatively in QCD [1], except at small x [2]. In practice, however, non-perturbative effects are found to be significant [3, 4] at present experiments, where the electromagnetic structure of Weizsäcker–Williams quasi-real photon [5] has been measured up to the momentum transfer scale $Q^2 = 100$ GeV^2 in e^+e^- collision experiments. Several parametrizations of the scale-dependent effective parton distributions in the photon have been proposed; some are based on plausible dynamical assumptions [3,6–9] and the others [4,10] have been obtained by fitting phenomenologically to the photon structure function data [11–17]. These parametrizations typically have similar quark distributions which are directly constrained by the structure function data. On the other hand, wildly different gluon distributions have been proposed since the electromagnetic structure of the photon is rather insensitive to its gluon content.

Recently TRISTAN experiments [18, 19] have shown evidence for the effective gluon content of the photon in two-photon production of high transverse momentum (p_T) jets. The observed jet production cannot be understood without the contribution from gluons in the colliding photons, whereas it does not allow a very hard gluon distribution [10] that is consistent with the structure function data.

More recently, the TRISTAN experiments have reported evidence for copious production of charmed particles in the two-photon collision process, in various modes and at various p_T range [20–22]. The charm production rate has been found to be particularly sensitive to the gluon distribution in the photon [23] and that the present data tend to prefer those parametrizations with large gluon content at small x ($x \lesssim 0.1$).

The present data on the jet and charm production in the two-photon process thus give us evidence and some quantitative information of the gluon content of the photon, but they are not yet accurate enough to determine directly the effective gluon distribution. It is therefore desirable to have a set of effective parton distributions in the photon with systematically different gluon distributions, so that we can learn more about the photon structure from these experiments.

In this report we study all the available photon structure function data [11–17,24–26] at 4 GeV$^2 \leq Q^2 \leq 100$ GeV^2 in the leading order of perturbative QCD and, find a

new set of the effective scale-dependent parton distributions in the photon, WHIT1 to WHIT6, which are all consistent with the present data of the photon structure function and have systematically different gluon contents. We study carefully the charm quark contributions to the observed structure functions, which are evaluated by using the lowest order quark parton model matrix elements ($\gamma^*\gamma \to c\bar{c}$ and $\gamma^* g \to c\bar{c}$), the massive AP equations [27, 28], and the massless four-flavor AP equations at different Q^2 range. We find that the photon structure function has a sensitivity to the gluon distribution at small x, but that a careful analysis is needed to determine experimentally the photon structure in this region. Predictions are also given for the total charm quark pair production cross section in the two-photon collision process at e^+e^- colliders.

We note here that the next-to-leading order correction to the massless inhomogeneous Altarelli–Parisi equations (IAPE) have been known for a while [3, 29–31], and some phenomenological analyses [6–9] were performed at this level. Recently, the complete next-to-leading order correction has been obtained for the massive quark production process [32]. We work in the leading order of QCD, nevertheless, since errors in the experimental data as well as the theoretical uncertainties associated with the gluon contents of the photon are so large that the leading order approach is more suited to discuss them systematically.

The report is organized as follows. In section 2, we review the IAPE that govern the effective parton distributions in the photon and introduce the notion of 'valence' and 'sea' components of the quark distributions. We discuss our parametrization of the initial quark and gluon distributions and study charm contributions to the structure function. In section 3, we introduce all available photon structure function data, give a criterion to remove several low x experimental data, and then make a global fit to the initial light-quark distribution functions by using the leading order AP equations. The fit is repeated by systematically changing the magnitude and the shape of the initial gluon distribution. The minimal χ^2 of the fit as well as the χ distribution of each data point are examined carefully. Six effective parton distributions, WHIT1 to WHIT6, are then introduced which have systematically different initial gluon distributions. In section 4 we compare our effective gluon distributions with some other typical parametrizations. Predictions are also given for the total charmed quark production cross section in the two-photon process at e^+e^- colliders. Section 5 summarizes our findings.

The details on the numerical methods that we used to solve the IAPE with and without

quark mass effects, and the parametrizations of our effective parton distributions in the photon will be given elsewhere [33].

2 Model

In this section we explain the framework adopted in this work to calculate the effective parton distribution functions in the photon and the photon structure function $F_2^\gamma(x, Q^2)$.

2.1 Inhomogeneous Altarelli–Parisi equations

In the Q^2 region where the lightest f-flavor quarks can be produced, we have f quark distributions and f anti-quark distributions in addition to the gluon distribution in the photon. These are denoted by $q_i(x, Q^2)$, $\bar{q}_i(x, Q^2)$ ($i = 1$ to f), and $g(x, Q^2)$ respectively. Apparently, the relation $q_i(x, Q^2) = \bar{q}_i(x, Q^2)$ holds for each flavor.

The Q^2 evolution of these parton distributions is described by the inhomogeneous Altarelli–Parisi equations (IAPE) in the leading logarithmic approximation [34]. For massless f-flavor case the IAPE can be written as follows:

$$\frac{dq_i(x, Q^2)}{dt} = \frac{\alpha}{2\pi} e_i^2 P_{q\gamma}(x) + \frac{\alpha_s(Q^2)}{2\pi} \left[P_{qq}(x) \otimes q_i(x, Q^2) + P_{qg}(x) \otimes g(x, Q^2) \right] , \quad \text{(1a)}$$

$$\frac{dg(x, Q^2)}{dt} = \frac{\alpha_s(Q^2)}{2\pi} \left[2P_{gq}(x) \otimes \sum_{i=1}^{f} q_i(x, Q^2) + P_{gg}(x, f) \otimes g(x, Q^2) \right] , \quad \text{(1b)}$$

where $i = 1$ to f, $t = \log Q^2/\Lambda^2$, and P_{ij}'s are the parton splitting functions whose explicit formulas are found in the literature [35]. The convolution integral is defined as $a(x) \otimes b(x) = \int_x^1 dy/y \, a(x/y) b(y)$.

As we show in the latter sections, the charm quark contribution to the photon structure function can be most conveniently calculated from the lowest order quark parton model processes ($\gamma^*\gamma \to c\bar{c}$ and $\gamma^* g \to c\bar{c}$) at present energies ($Q^2 \lesssim 100$ GeV^2), by excluding the charm quark distribution in the photon. Only at higher Q^2 we introduce the effective charm quark distribution that evolves according to the massless $f = 4$ IAPE of eq. (1a). The matching of the quark parton model description and that with the effective heavy quark distribution is discussed in ref. [33].

Hence in the analysis of the present structure function data, we introduce only three light quark distributions ($f = 3$). Furthermore, in order to find a plausible parametrization

of these quark distributions for the fit, we find it convenient to introduce the notion of *valence* and *sea* quark distributions. The *valence* quarks are produced by the photon and the *sea* quarks originate from the gluons. According to these definitions, the valence and sea quark distributions are written in terms of the original quark distributions q_i's:

$$q_v(x,Q^2) = 2\sum_{i=1}^{3} \frac{e_i^2\langle e^2\rangle - \langle e^2\rangle^2}{\langle e^4\rangle - \langle e^2\rangle^2} q_i(x,Q^2)\,, \tag{2a}$$

$$q_{sea}(x,Q^2) = 2\sum_{i=1}^{3} \frac{\langle e^4\rangle - e_i^2\langle e^2\rangle}{\langle e^4\rangle - \langle e^2\rangle^2} q_i(x,Q^2)\,, \tag{2b}$$

where $\langle e^2\rangle = 2/9$ and $\langle e^4\rangle = 2/27$ for $f = 3$. Note that the popular singlet and non-singlet quark distributions are related to our valence and sea quark distributions by

$$\begin{aligned} q_S(x,q^2) &\equiv 2\sum_{i=1}^{3} q_i(x,Q^2)\,, \\ &= q_v(x,Q^2) + q_{sea}(x,Q^2)\,, \end{aligned} \tag{3a}$$

$$\begin{aligned} q_{NS}(x,Q^2) &\equiv 2\sum_{i=1}^{3} \left[e_i^2 - \langle e^2\rangle\right] q_i(x,Q^2)\,, \\ &= \left[\frac{\langle e^4\rangle}{\langle e^2\rangle} - \langle e^2\rangle\right] q_v(x,Q^2)\,, \end{aligned} \tag{3b}$$

where $q_S(x,q^2)$ and $q_{NS}(x,q^2)$ are the singlet and non-singlet quark distributions respectively.

The photon structure function $F_2^\gamma(x,Q^2)$ can be written in terms of $q_v(x,Q^2)$ and $q_{sea}(x,Q^2)$ as

$$\begin{aligned} F_2^\gamma(x,Q^2) &\equiv 2x\sum_{i=1}^{f} e_i^2 q_i(x,Q^2)\,, \\ &= x\left[\frac{\langle e^4\rangle}{\langle e^2\rangle} q_v(x,Q^2) + \langle e^2\rangle q_{sea}(x,Q^2)\right] + \text{heavy quarks}\,. \end{aligned} \tag{4}$$

Heavy quark contributions will be discussed in subsection 2.3. When we neglect small mass differences among the light three flavors, we can express the u, d and s distributions in terms of q_v and q_{sea}:

$$u(x,Q^2) = \frac{1}{3} q_v(x,Q^2) + \frac{1}{6} q_{sea}(x,Q^2)\,, \tag{5a}$$

$$d(x,Q^2) = s(x,Q^2) = \frac{1}{12} q_v(x,Q^2) + \frac{1}{6} q_{sea}(x,Q^2)\,. \tag{5b}$$

The IAPE in eq. (1) can be rewritten in terms of the valence quark, the sea quark and the gluon distributions:

$$\frac{dq_v(x,Q^2)}{dt} = \frac{\alpha}{2\pi}\langle e^2\rangle P_{q\gamma}(x) + \frac{\alpha_s(Q^2)}{2\pi} P_{qq}(x) \otimes q_v(x,Q^2)\,, \tag{6a}$$

$$\frac{dq_{sea}(x,Q^2)}{dt} = \frac{\alpha_s(Q^2)}{2\pi}\left[P_{qq}(x) \otimes q_{sea}(x,Q^2) + 2\cdot 3P_{qg}(x) \otimes g(x,Q^2)\right]\,, \tag{6b}$$

$$\frac{dg(x,Q^2)}{dt} = \frac{\alpha_s(Q^2)}{2\pi}\left[P_{gq}(x) \otimes \left\{q_v(x,Q^2) + q_{sea}(x,Q^2)\right\} + P_{gg}(x,3) \otimes g(x,Q^2)\right]. \tag{6c}$$

Once a set of initial parton distributions at $Q^2 = Q_0^2$ is given, we can predict the parton distributions at any $Q^2(> Q_0^2)$ by solving the above equations numerically. The numerical methods which we used is explained in appendix A of ref. [33].

2.2 Initial parton distributions

To solve the IAPE in eq. (6), we have to specify a set of initial parton distributions at $Q^2 = Q_0^2$. All the non-perturbative features of the photon structure are included in these initial conditions. We use $Q_0^2 = 4$ GeV^2 throughout our analysis in order that our perturbation approximation works well.

As an initial valence quark distribution, we take the following functional form:

$$xq_v(x,Q_0^2)/\alpha = A_v x^{B_v}(1-x)^{C_v}/B(B_v+1, C_v+1)\,, \tag{7}$$

where A_v, B_v and C_v are the free parameters which will be fitted to the experimental data, and $B(\alpha,\beta)$ is the beta function that ensures the normalization,

$$\langle xq_v(x,Q_0^2)\rangle/\alpha = \int_0^1 xq_v(x,Q_0^2)/\alpha\, dx = A_v\,, \tag{8}$$

for the energy fraction $\langle xq_v(x,Q_0^2)\rangle$ of the valence quark in the photon.

As for the initial gluon distribution, we adopt the simple form

$$xg(x,Q_0^2)/\alpha = A_G(C_G+1)(1-x)^{C_G}\,, \tag{9}$$

with two parameters, A_G and C_G. Again the normalization factor is chosen such that $\langle xg(x,Q_0^2)\rangle/\alpha = A_G$. The present structure function data are not accurate enough to determine the gluon parameters A_G and C_G. We therefore perform the fit on the valence quark parameters, A_v, B_v and C_v, by varying systematically the normalization (A_G) and the shape (C_G) of the initial gluon distribution.

Before starting the fit to the data, we discuss plausible range of the gluon distribution parameters that we should explore. We obtain a plausible constraint [7] on the ratio of the gluon energy fraction (A_G) to the valence quark energy fraction (A_v) as follows. At sufficiently low momentum transfer scale ($Q^2 \lesssim 0.5$ GeV^2), only the long wavelength components of the photon are probed and the quark-antiquark pair produced from the photon undergoes non-perturbative soft QCD dynamics that resembles the one which make them from the low-lying vector boson. The photon structure is then expected to have components similar to those of the vector boson, in particular the ρ meson that couples strongly to the photon. Although we do not know the structure of ρ, we expect the soft QCD dynamics to be insensitive to the total spin of the system and that it may be similar to the observed π structure [36]. If the photon had only this soft component, its deep structure should also be similar and we expect

$$\frac{\langle xg(x,Q_0^2)\rangle_{`\rho'}}{\langle xq_v(x,Q_0^2)\rangle_{`\rho'}} \sim \frac{\langle xg(x,Q_0^2)\rangle_\pi}{\langle xq_v(x,Q_0^2)\rangle_\pi} \sim 1\,. \tag{10}$$

In fact this ratio is common in the nucleon structure as well [28, 37] and we can regard this ratio as an universal one from soft QCD dynamics.

The photon, however, differs from the vector boson in that it is a source of a quark-pair with an arbitrary short wave-length. As the momentum transfer scale grows ($Q^2 \gtrsim 0.5$ GeV^2), one is more and more sensitive to these short wave-length components which dominate the photon structure at asymptotically high Q^2. Although the transition from the regime where the vector meson-like component dominates to the regime where the short wave-length component dominates is gradual and it is governed by the non-perturbative dynamics, we may infer the effect of the latter component from its asymptotic behavior that can be calculated perturbatively. In particular, for the ratio of the gluon to valence quark energy fraction, we expect

$$\left.\frac{\langle xg(x,Q^2)\rangle}{\langle xq_v(x,Q^2)\rangle}\right|_{Q^2\to\infty} = \frac{3616}{10611} \simeq \frac{1}{3}\,, \tag{11}$$

for three light quark flavors ($f = 3$). At the momentum transfer scale $Q_0^2 = 4$ GeV^2, it is hence natural to expect the ratio to lie somewhere between the two extremes (10) and (11):

$$\frac{1}{3} \lesssim \frac{\langle xg(x,Q_0^2)\rangle}{\langle xq_v(x,Q_0^2)\rangle} = \frac{A_G}{A_v} \lesssim 1\,. \tag{12}$$

We shall see in the next section that the valence quark fraction A_v is determined to be about unity by the experimental data of $F_2^\gamma(x, Q^2)$. We will hence examine the parameter range $1/3 \lesssim A_G \lesssim 1$ for the gluon energy fraction.

Finally, we note that the sea quark distribution is intimately related to the gluon distribution and that we cannot choose them independently. Although the sea quark distribution is in principle observable as the small x behavior of the structure function, we find that the experimental determination of the small x structure suffers from an uncertainty associated with the extrapolation technique [38] adopted by most experiments: this will be discussed in the section 3. We therefore estimate the input sea quark distribution by using the quark parton model cross section for the process $\gamma^* g \to q\bar{q}$:

$$xq_{sea}(x, Q_0^2) = 3\,\frac{\alpha_s(Q_0^2)}{2\pi}\int_{ax}^{1} dy\, w\left(\frac{x}{y}, \frac{m^2}{Q_0^2}\right) g(y, Q_0^2)\,, \tag{13}$$

where $a = 1 + 4m^2/Q_0^2$ and

$$\begin{aligned} w(z, r) = z\,\Big[&\beta\,\{-1 + 8z(1-z) - 4rz(1-z)\} \\ &+ \left\{z^2 + (1-z)^2 + 4rz(1-3z) - 8r^2z^2\right\}\log\frac{1+\beta}{1-\beta}\Big] \end{aligned} \tag{14}$$

with $\beta = \sqrt{1 - 4rz/(1-z)}$. The sea quark mass m, which is taken to be common for the three light flavors, $m_u = m_d = m_s = m$, plays the role of the cut-off and we choose it to be 0.5 GeV. Here and throughout our analysis we adopt the leading order form of the QCD running coupling constant

$$\frac{\pi}{\alpha_s(Q^2)} = \frac{25}{12}\ln\frac{Q^2}{\Lambda^2} - \frac{1}{6}\ln\frac{Q^2}{4m_b^2}\theta(Q^2 - 4m_b^2)\,, \tag{15}$$

with $\Lambda = 0.4$ GeV. Note that the effective number of quark flavors that governs the running of the coupling constant is chosen independently of the number f of massless quark flavors in the IAPE of eq. (1). An accurate prescription is found only in the next-to-leading order level [32].

We remark here that the above prescription leads naturally to larger sea quark input as the gluon input is enhanced. In particular, we find for the energy fraction ratio that

$$\frac{\langle xq_{sea}(x, Q_0^2)\rangle}{\langle xg(x, Q_0^2)\rangle} \sim 0.12 \tag{16}$$

holds almost independent of the input gluon parameters A_G and C_G. The ratio increases with decreasing light quark mass, and reaches 0.2 at $m \sim 0.3$ GeV. The ratio is about 0.3 in the parametrization of the π structure [36], and its asymptotic value is calculated to be 0.16 for $f = 3$. Our sea quark input is hence rather conservative for a given input gluon distribution.

2.3 Charm contribution

The charm quark cannot be incorporated into the massless IAPE in the region of moderate Q^2, say $Q^2 < 100$ GeV^2, which has so far been probed by experiments. We should take into account the quark mass effect by using the massive-quark AP equation of Glück *et al.* [27,28], and more accurately by incorporating the full next-to-leading order corrections [32]. We find by comparing with the results of the leading order massive-quark IAPE that at $Q^2 < 100$ GeV^2 the charm quark contribution to the photon structure function is well approximated by the sum of the contributions from the quark parton model processes $\gamma^*\gamma \to c\bar{c}$ and $\gamma^* g \to c\bar{c}$. At higher Q^2, the charm quark mass effect to the Q^2-evolution becomes negligible and that we can use the massless IAPE of eq. (1) with $f = 4$. The matching of the distributions can be made at any points around $Q^2 \sim 100$ GeV^2. With the same criterion, we find that the bottom quark contribution can be estimated by the lowest order process $\gamma^*\gamma \to b\bar{b}$ and $\gamma^* g \to b\bar{b}$ up to about $Q^2 \sim 1000$ GeV^2, above which we may introduce the effective b-quark distribution that follows the massless $f = 5$ IAPE. More accurate quantitative treatment [32] will become useful in the future when both the quark and gluon distributions are measured accurately from experiments.

The contribution of the direct process ($\gamma^*\gamma \to c\bar{c}$) is given by

$$F^{\gamma}_{2,c}(x, Q^2)|_{\text{direct}} = 3\frac{\alpha}{\pi} e_c^4 \, w\left(x, \frac{m_c^2}{Q^2}\right) , \tag{17}$$

where $e_c = 2/3$ is the charm electric charge and the function $w(x, r)$ is given in eq. (14). In our numerical analysis, we take $m_c = 1.5$ GeV. For the resolved process ($\gamma^* g \to c\bar{c}$) , we have

$$F^{\gamma}_{2,c}(x, Q^2)|_{\text{resolved}} = \frac{\alpha_s(Q^2)}{2\pi} e_c^2 \int_{ax}^{1} dy \, w\left(\frac{x}{y}, \frac{m_c^2}{Q^2}\right) g(y, Q^2) , \tag{18}$$

where $a = 1 + 4m_c^2/Q^2$, and the gluon distribution $g(x, Q^2)$ is given by solving the massless $f = 3$ IAPE in eq. (6) with the initial parton distributions in eqs. (7), (9) and (13).

Table 1: The data adopted in the fit of the valence quark parameters.

collider	collab.	$\langle Q^2 \rangle$	x bins	Ref.
PETRA	PLUTO	4.3 GeV^2	0.03–0.17, 0.17–0.44, 0.44–0.80	[11]
		9.2 GeV^2	0.06–0.23, 0.23–0.54, 0.54–0.90	[11]
		45.0 GeV^2	0.25–0.50, 0.50–0.75, 0.75–0.90	[12]
	TASSO	23.0 GeV^2	0.20–0.40, 0.40–0.60, 0.60–0.80, 0.80–0.98	[13]
	JADE	24.0 GeV^2	0.10–0.20, 0.20–0.40, 0.40–0.60, 0.60–0.90	[14]
		100.0 GeV^2	0.10–0.30, 0.30–0.60, 0.60–0.90	[14]
PEP	TPC/2γ	5.1 GeV^2	0.02–0.20, 0.20–0.36, 0.36–0.74	[15]
		20.0 GeV^2	0.196–0.386, 0.386–0.611, 0.611–0.963	[16]
TRISTAN	AMY	73.0 GeV^2	0.125–0.375, 0.375–0.625, 0.625–0.875	[17]
	TOPAZ	5.1 GeV^2	0.076–0.20	[24]
		16.0 GeV^2	0.15–0.33, 0.33–0.78	[24]
		80.0 GeV^2	0.32–0.59, 0.59–0.98	[24]
	VENUS	40.0 GeV^2	0.09–0.27, 0.27–0.45, 0.45–0.63, 0.63–0.81	[25]
		90.0 GeV^2	0.19–0.37, 0.37–0.55, 0.55–0.73, 0.73–0.91	[25]
LEP	OPAL	5.9 GeV^2	0.091–0.283, 0.283–0.649	[26]
		14.7 GeV^2	0.137–0.324, 0.324–0.522, 0.522–0.836	[26]

The validity of our simple perturbative calculation depends on how much the gluon emission by the charm quark distorts the charm quark distribution in the photon. The magnitude of this effect can be studied by using the massive IAPE for the charm quark and is presented in ref. [33].

3 Fit to the data

3.1 Data

In order to find good initial parton distributions at the energy scale $Q_0^2 = 4.0$ GeV^2, we refer to the all available experimental data of the photon structure function at $Q^2 > Q_0^2$. The photon structure function has been measured mainly at e^+e^- colliders. In our analysis we use data from 8 groups which are listed in Table 1. These data in the table are almost all published, while some have been presented at the this workshop.

We note here that not all the published experimental data are taken into account in our fit. First, we do not use the data at $\langle Q^2 \rangle$ lower than 4.0 GeV^2. Second, we remove

from our fit those data points at small x where the following inequality holds:

$$x_{\text{lower edge of the bin}} < \frac{\langle Q^2 \rangle}{\langle Q^2 \rangle + (W_{\text{vis}}^{\max})^2} \tag{19}$$

Here $W_{\text{vis}}^{\max}$ is the experimental cut on the visible invariant mass of the final hadron system. Since those data points are obtained at near the boundary of the experimental acceptance and since the sea quark contribution can be rather singular at the low x region, these data may have large systematic error in the unfolding procedure [38]. As a result of the above two requirements, 47 data points are retained in our fitting, which are all listed in Table 1.

3.2 Fit

By fitting our theoretical solution of the photon structure function to these experimental data, we tune the parameters of the initial valence quark distribution A_v, B_v and C_v. We repeat the fit by varying the initial gluon distribution parameters A_G and C_G systematically. In particular, we examine the case with $A_G = 0.5$ and $A_G = 1$ and find little sensitivity of the structure function data. The fit results for arbitrarily chosen six cases are summarized in Table 2. We name these six gluon inputs as WHIT1 to WHIT6.

Fig. 1 illustrates the matching of the data and the theoretical curves, and Fig. 2 shows the χ distributions of each data point. As seen in Fig. 1, all of WHIT1 to WHIT6 give similar quality of fit to the photon structure function data. From Table 2, it is found that the χ^2 of the best fit depends only mildly on the choice of the initial gluon distribution parameters. It means that the present experimental data on the photon structure function have poor sensitivity to the gluonic content of the photon. The normalization of the valence quark distribution A_v is found to be roughly 1, regardless of the difference in the sea quark contribution that depends on our gluon inputs.

We find that the best values of the initial valence quark parameters are almost the same for different C_G for a common A_G. Thus we set the 'standard' set of the valence quark parameters for each A_G; *i.e.*

$$A_G = 0.5 \ : \ A_v = 0.94 \ , \quad B_v = 0.50 \ , \quad C_v = 0.25 \ , \tag{20a}$$

$$A_G = 1.0 \ : \ A_v = 0.89 \ , \quad B_v = 0.70 \ , \quad C_v = 0.45 \ . \tag{20b}$$

We repeat the fit for various C_G by fixing the normalization A_G and the associated valence quark inputs as above, and the result is summarized in able 3. The C_G dependence of

Table 2: The χ^2 and the valence quark parameters obtained by the best fit.

name	gluon		best fit	valence quark parameters			correlations		
	A_G	C_G	χ^2	A_v	B_v	C_v	$\rho(A_v,B_v)$	$\rho(A_v,C_v)$	$\rho(B_v,C_v)$
WHIT1	0.5	3	51.6	0.930(79)	0.50(17)	0.24(25)	−0.52	−0.75	0.88
WHIT2	0.5	9	54.0	0.938(78)	0.49(16)	0.28(25)	−0.52	−0.75	0.88
WHIT3	0.5	15	54.3	0.948(78)	0.44(16)	0.26(25)	−0.52	−0.75	0.88
WHIT4	1.0	3	54.0	0.873(76)	0.77(21)	0.41(29)	−0.52	−0.73	0.88
WHIT5	1.0	9	60.2	0.892(74)	0.71(19)	0.47(29)	−0.53	−0.74	0.88
WHIT6	1.0	15	60.4	0.911(75)	0.61(17)	0.42(28)	−0.53	−0.75	0.88

Table 3: The χ^2 with the standard valence quark parameters.

name	gluon			name	gluon		
	A_G	C_G	χ^2		A_G	C_G	χ^2
	0.5	1	50.7		1.0	1	54.2
	0.5	2	51.1		1.0	2	55.0
WHIT1	0.5	3	51.6	WHIT4	1.0	3	56.0
	0.5	4	52.2		1.0	4	57.0
	0.5	5	52.7		1.0	5	57.9
	0.5	6	53.2		1.0	6	58.6
	0.5	7	53.6		1.0	7	59.3
	0.5	8	54.0		1.0	8	59.8
WHIT2	0.5	9	54.3	WHIT5	1.0	9	60.2
	0.5	10	54.5		1.0	10	60.6
	0.5	11	54.7		1.0	11	60.9
	0.5	12	54.9		1.0	12	61.1
	0.5	13	55.1		1.0	13	61.2
	0.5	14	55.2		1.0	14	61.3
WHIT3	0.5	15	55.3	WHIT6	1.0	15	61.4
	0.5	16	55.3		1.0	16	61.5

the obtained χ^2 is also represented in Fig. 3. We adopt the valence quark input (20a) for the sets WHIT1 to WHIT3, while that of (20b) for the sets WHIT4 to WHIT6. The slightly small valence quark contribution of (20b) at small x compensates for larger sea quark contribution associated with the large gluon inputs of WHIT4 to WHIT6.

4 Discussions

4.1 Gluon distribution

Our effective gluon distributions in the sets WHIT1 to WHIT6 are compared with that of Drees and Grassie (DG) [4] and Abramowicz, Charchuła and Levy (LAC1) [10] parametrizations at three momentum transfer scales in Fig. 4. All gluon distributions become similar at high Q^2, as expected from the asymptotic behavior of the solution of the IAPE.

It is notable that our WHIT6 parametrization gives the similar gluon distribution with LAC1 in the x range shown in this figure, although the LAC1 gluon is more singular at $x \to 0$, which results in too large energy fraction $\langle xg(x, Q_0^2)\rangle/\alpha = 2.37$ at $Q_0^2 = 4$ GeV^2.

4.2 Charm production cross section

Here we study the charm production cross section via the two-photon processes by using our new parton distribution functions in the photon. The charm quark production cross section is expected to be much more sensitive on the gluonic content of the photon than the structure function [23]. Fig. 5 illustrates a rough estimate on the charm quark production cross section. They are obtained for $m_c = 1.5$ GeV and fixed QCD coupling $\alpha_s(Q^2) = \alpha_s(4m_c^2)$ with $\Lambda = 0.4$ GeV. Uncertainties in these predictions are discussed in ref. [33, 39]. As can be seen from the figure, TRISTAN experiments differ significantly from the experiments at lower energy scales, and they are expected to be quite sensitive to the gluon distribution in the photon. Similar results can be expected on the p_T distribution of the produced charm quark.

5 Conclusions

We have studied all the available photon structure function data [11–17, 24–26] at 4 GeV$^2 \leq Q^2 \leq 100$ GeV^2 in the leading order of perturbative QCD and, have found a

new set of the effective scale-dependent parton distributions in the photon, WHIT1 to WHIT6, which are all consistent with the present data of the photon structure function and have systematically different gluon contents. We have studied carefully the charm quark contributions to the observed structure functions, which are evaluated by using the lowest order quark parton model matrix elements ($\gamma^*\gamma \to c\bar{c}$ and $\gamma^* g \to c\bar{c}$), the massive AP equations, and the massless four-flavor AP equations at different Q^2 range. We have found that the photon structure function has a sensitivity to the gluon distribution at small x, but that a careful analysis is needed to determine experimentally the photon structure in this region. Predictions have been also given for the total charm quark pair production cross section in the two-photon collision process at e^+e^- colliders.

Acknowledgment

I would like to thank K. Hagiwara (KEK), M. Tanaka (KEK) and T. Izubuchi (Univ. of Tokyo) for collaboration that has led us to the results presented here. I am grateful to our experimental colleagues, T. Nozaki of AMY, T. Tauchi and H. Hayashii of TOPAZ and S. Odaka, H. Ohyama and T. Oyama of VENUS collaborations, for keeping us informed about the latest analysis of their data. I thank M. Drees and P. M. Zerwas for valuable discussions on the charm quark production cross section. I also thank S. Matsumoto for providing us with an efficient computer program to perform the χ^2 fit.

References

[1] E. Witten, Nucl. Phys. **B120**, 1977) 189.

[2] W. A. Bardeen and A. J. Buras, Phys. Rev. **D20** (1979) 166; erratum, **D21** (1980) 2041; D. W. Duke and J. F. Owens, Phys. Rev. **D22** (1980) 2280; G. Rossi, Phys. Lett. **B130** (1983) 105; I. Antoniadis and G. Grunberg, Nucl. Phys. **B213** (1983) 445.

[3] M. Glück and E. Reya, Phys. Rev. **D28** (1983) 2749.

[4] M. Drees and K. Grassie, Z. Phys. **C28** (1985) 451.

[5] C. Weizäcker, Z. Phys. **88** (1934) 612; E. J. Williams, Phys. Rev. **45** (1934) 729.

[6] J. H. Field, F. Kapusta and L. Piggioli, Phys. Lett. **B181** (1986) 362; Z. Phys. **C36** (1987) 121.

[7] L. E. Gordon and J. K. Storrow, Z. Phys. **C56** (1992) 307.

[8] P. Aurenche, P. Chiappetta, M. Fontannaz, J. P. Guillet and E. Pilon, Z. Phys. **C56** (1992) 589.

[9] M. Glück, E. Reya and A. Vogt, Phys. Rev. **D46** (1992) 1973.

[10] H. Abramowicz, K. Charchuła and A. Levy, Phys. Lett. **B269** (1991) 458.

[11] PLUTO collab., Ch. Berger *et al.*, Phys. Lett. **B142** (1984) 111.

[12] PLUTO collab., Ch. Berger *et al.*, Nucl. Phys. **B281** (1987) 365.

[13] TASSO collab., M. Althoff *et al.*, Z. Phys. **C31** (1986) 527.

[14] JADE collab., W. Bartel *et al.*, Z. Phys. **C24** (1984) 231.

[15] TPC/Two-Gamma collab., H. Aihara *et al.*, Z. Phys. **C34** (1987) 1.

[16] TPC/Two-Gamma collab., J. S. Steinman, UCLA preprint, UCLA-HEP-88-004 (1988).

[17] AMY collab., T. Sasaki *et al.*, Phys. Lett. **B252** (1990) 491.

[18] AMY collab., R. Tanaka *et al.*, Phys. Lett. **B277**, 215 (1992).

[19] TOPAZ collab., H. Hayashii *et al.*, Phys. Lett. **B314**, 149 (1993).

[20] TOPAZ collab., R. Enomoto *et al.*, KEK Preprint 93-107 (1993).

[21] VENUS collab., S. Uehara *et al.*, KEK Preprint 93-142 (1993).

[22] AMY collab., T. Aso, talk in this workshop.

[23] M. Drees and R. M. Godbole, Nucl. Phys. **B339** (1990) 355.

[24] TOPAZ collab., H. Muramatsu, talk given in this workshop.

[25] VENUS collab., T. Oyama *et al.*, private communication.

[26] OPAL collab., R. Akers *et al.*, CERN preprint, CERN-PPE/93-156.

[27] M. Glück, E. Hoffmann, and E. Reya, Z. Phys. **C13** (1982) 119.

[28] E. Eichten, I. Hinchliffe, K. Lane and C. Quigg, Rev. of Mod. Phys. **56** (1984) 579.

[29] W. A. Bardeen and A. J. Buras, in [2].

[30] M. Glück, E. Reya and A. Vogt, Phys. Rev. **D45** (1991) 3986.

[31] M. Fontannaz and E. Pilon, Phys. Rev. **D45** (1992) 382.

[32] E. Laenen, S. Riemersma, J. Smith and W. L. van Neerven, Stony Brook preprint, ITP-SB-93-1 (1993); ITP-SB-93-46 (1993).

[33] K. Hagiwara, T. Izubuchi, M. Tanaka and I. Watanabe, KEK preprint, KEK-TH-376.

[34] R. J. DeWitt, L. M. Jones, J. D. Sullivan, D. E. Willen, and H. W. Wyld, Jr., Phys. Rev. **D19** (1979) 2046.

[35] G. Altarelli and G. Parisi, Nucl. Phys. **B126** (1977) 298; G. Altarelli, Phys. Rep. **81** (1982) 1.

[36] P. Aurenche, R. Baier, M. Fontannaz, M. N. Kienzle-Focacci and M. Werlen, Phys. Lett. **B233** (1989) 517.

[37] D. W. Duke and J. F. Owens, Phys. Rev. **D30** (1984) 49.

[38] JADE collab., W. Bartel *et al.*, in ref. [14]; V. Blodbel, in Proc. of the CERN School of Computing, Aiguablanca, Spain, September 1984, CERN 85-09, pp. 88, ed. C. Verkerk (1985); A. Bäcker, in Proc. of the 6th International Workshop on Photon-Photon Collisions, Cranlibakken, September 1984, pp. 205, ed. R. L. Lander (World Scientific, Singapore, 1985).

[39] M. Drees, M. Krämer, J. Zunft and P. M. Zerwas, Phys. Lett. **B306** (1993) 371.

Figure Captions

Fig. 1. The data and the theoretical predictions of the photon structure function F_2^γ. The vertical axes show F_2^γ and the horizontal axes represent the momentum fraction x. The data points with a cross mark are not used for the fit. (a) WHIT1–WHIT3. (b) WHIT4–WHIT6.

Fig. 2. The plots of χ of each data points. The data points with smaller x value are arranged lower in each data set with the common $\langle Q^2 \rangle$. The data points with a simple cross mark are not used for the fit.

Fig. 3. The C_G dependence of χ^2. Two curves are correspond χ^2's with the standard valence quark distribution, for $A_G = 0.5$ (solid) and 1.0 (dashed), respectively. The large plot marks are with the valence quark distribution at the best fit.

Fig. 4. The typical gluon distributions WHIT 1 to 6, DG and LAC1. The top 3 figures are for WHIT4 (solid), WHIT5 (dotted) and WHIT6 (dashed), the center 3 figures are WHIT1 (solid), WHIT2 (dotted) and WHIT3 (dashed), and the bottom 3 figures are DG (solid) and LAC1 (dashes) for comparison. The energy scale are at $Q^2 = 4$, 20 and 100 GeV^2 from left to right, respectively.

Fig. 5. The charm quark production cross section via the two-photon processes. The dot-dashed line corresponds the cross section due to the direct process only, while the other curves are sum of the direct process and the resolved process with different gluon distributions.

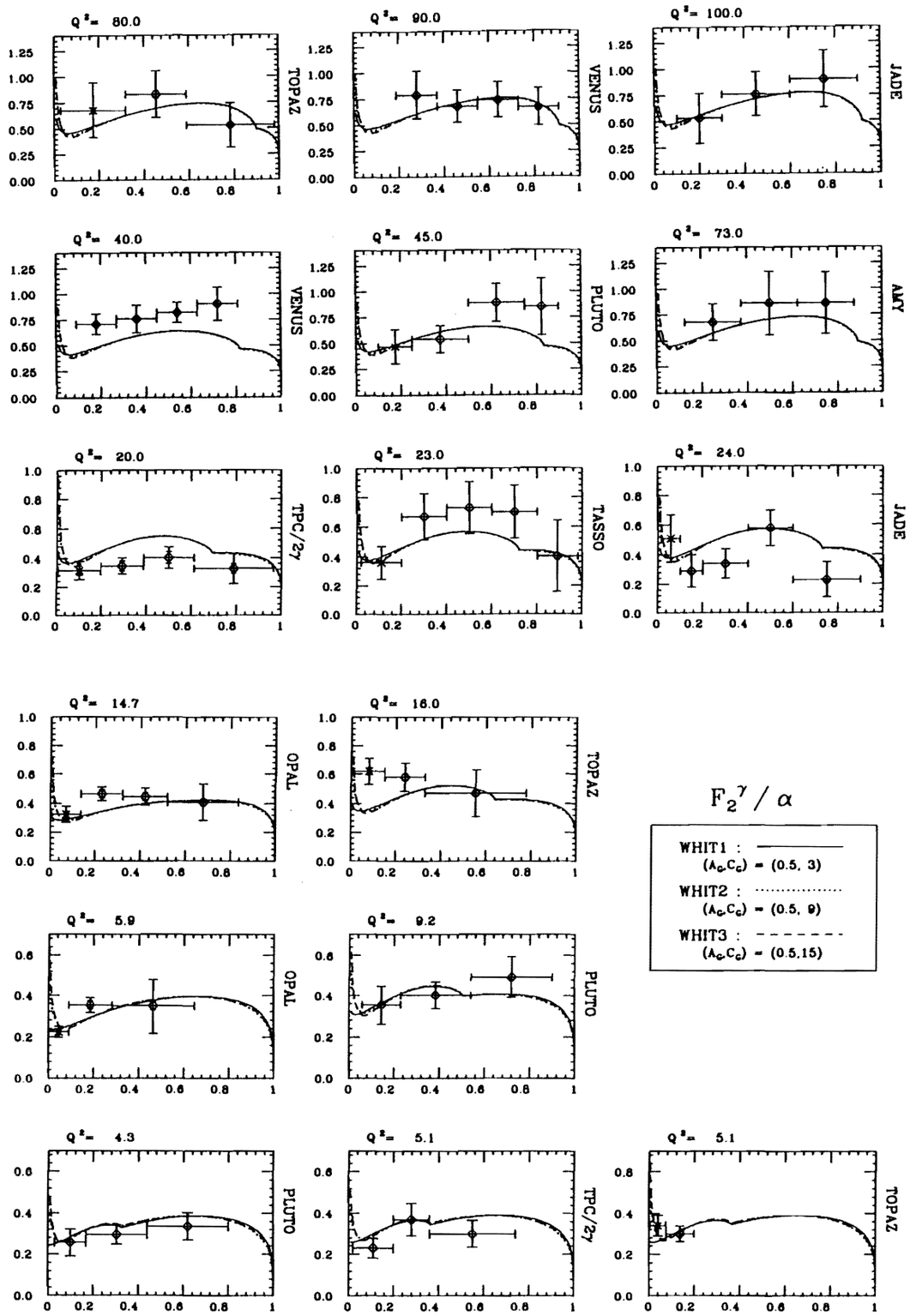
Q²= 100.0
JADE
Q²= 90.0
VENUS
Q²= 80.0
TOPAZ
Q²= 73.0
AMY
Q²= 45.0
PLUTO
Q²= 40.0
VENUS
Q²= 24.0
JADE
Q²= 23.0
TASSO
Q²= 20.0
TPC/2γ
Q²= 16.0
TOPAZ
Q²= 14.7
OPAL
Q²= 9.2
PLUTO
Q²= 5.9
OPAL
Q²= 5.1
TOPAZ
Q²= 5.1
TPC/2γ
Q²= 4.3
PLUTO
F₂γ / α
WHIT1 : (Λc,Cc) = (0.5, 3)
WHIT2 : (Λc,Cc) = (0.5, 9)
WHIT3 : (Λc,Cc) = (0.5,15)

Fig. 1(a)

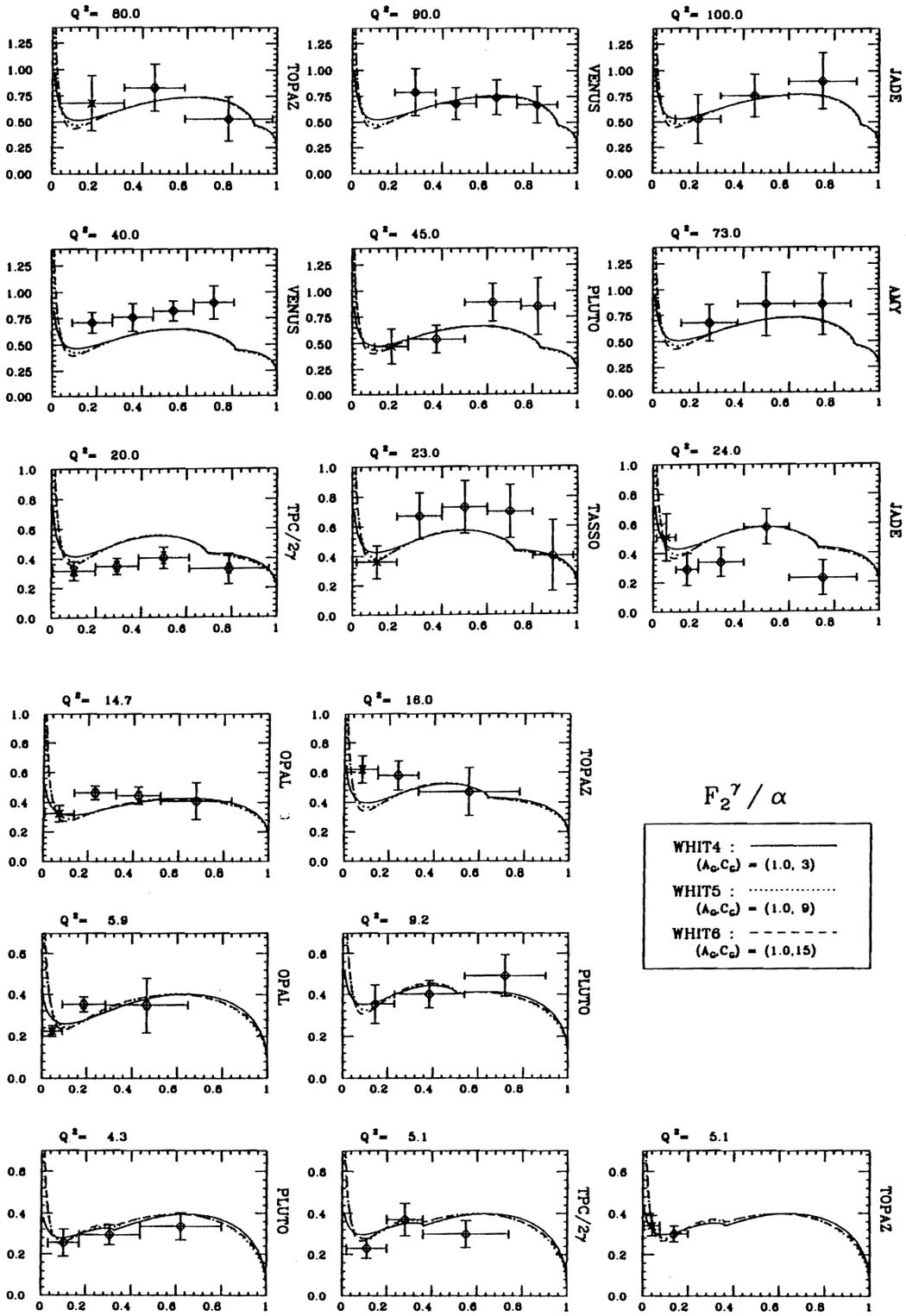
Q²= 80.0
TOPAZ
Q²= 90.0
VENUS
Q²= 100.0
JADE
Q²= 40.0
VENUS
Q²= 45.0
PLUTO
Q²= 73.0
AMY
Q²= 20.0
TPC/2γ
Q²= 23.0
TASSO
Q²= 24.0
JADE
Q²= 14.7
OPAL
Q²= 16.0
TOPAZ
Q²= 5.9
OPAL
Q²= 9.2
PLUTO
Q²= 4.3
PLUTO
Q²= 5.1
TPC/2γ
Q²= 5.1
TOPAZ
F₂^γ / α
WHIT4 :
(A_c,C_c) = (1.0, 3)
WHIT5 :
(A_c,C_c) = (1.0, 9)
WHIT6 :
(A_c,C_c) = (1.0,15)

Fig. 1(b)

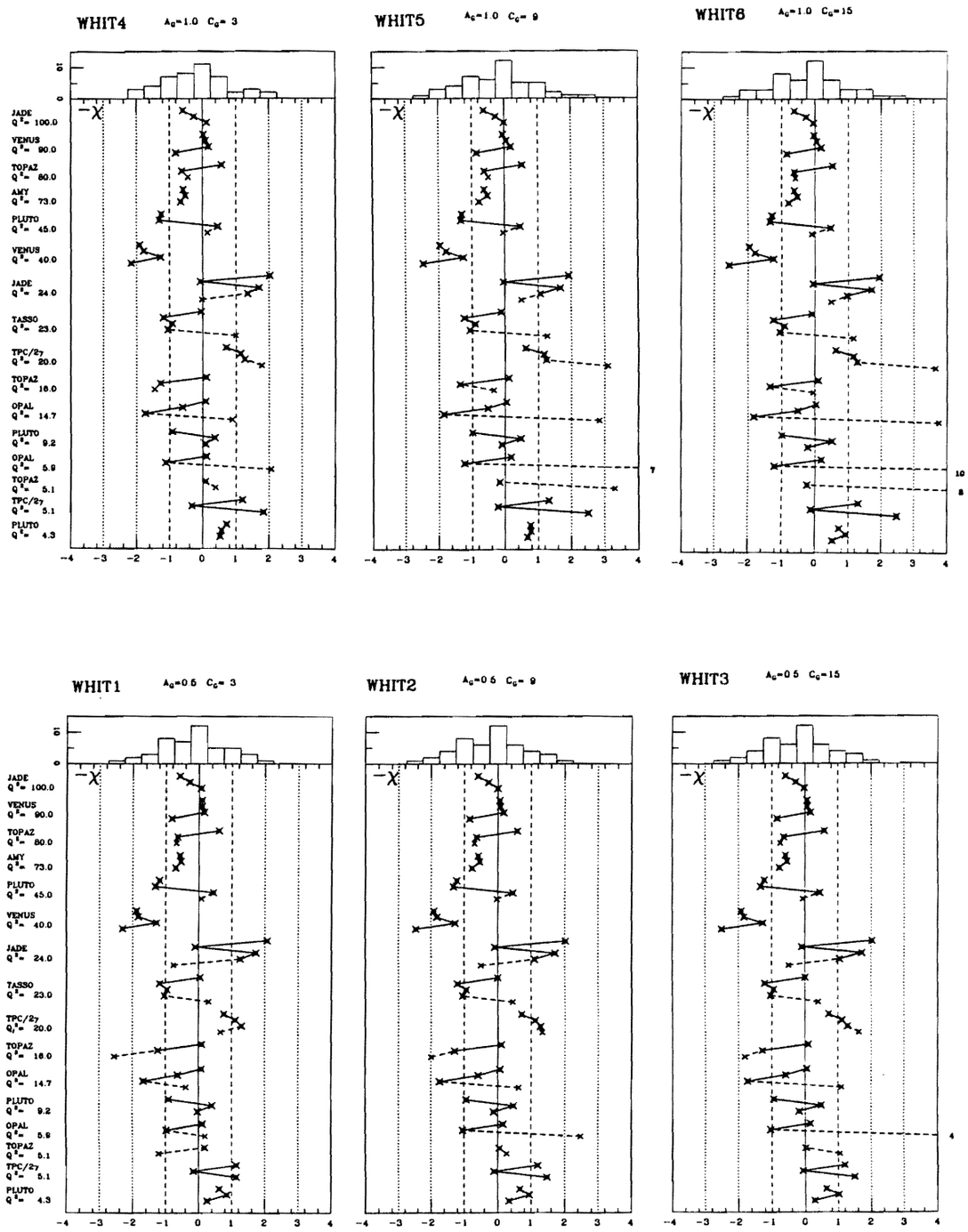
WHIT4 A_G=1.0 C_G= 3
WHIT5 A_G=1.0 C_G= 9
WHIT6 A_G=1.0 C_G=15
WHIT1 A_G=0.5 C_G= 3
WHIT2 A_G=0.5 C_G= 9
WHIT3 A_G=0.5 C_G=15
−χ
JADE Q^2= 100.0
VENUS Q^2= 90.0
TOPAZ Q^2= 80.0
AMY Q^2= 73.0
PLUTO Q^2= 45.0
VENUS Q^2= 40.0
JADE Q^2= 24.0
TASSO Q^2= 23.0
TPC/2γ Q^2= 20.0
TOPAZ Q^2= 18.0
OPAL Q^2= 14.7
PLUTO Q^2= 9.2
OPAL Q^2= 5.9
TOPAZ Q^2= 5.1
TPC/2γ Q^2= 5.1
PLUTO Q^2= 4.3
−4 −3 −2 −1 0 1 2 3 4

Fig. 2

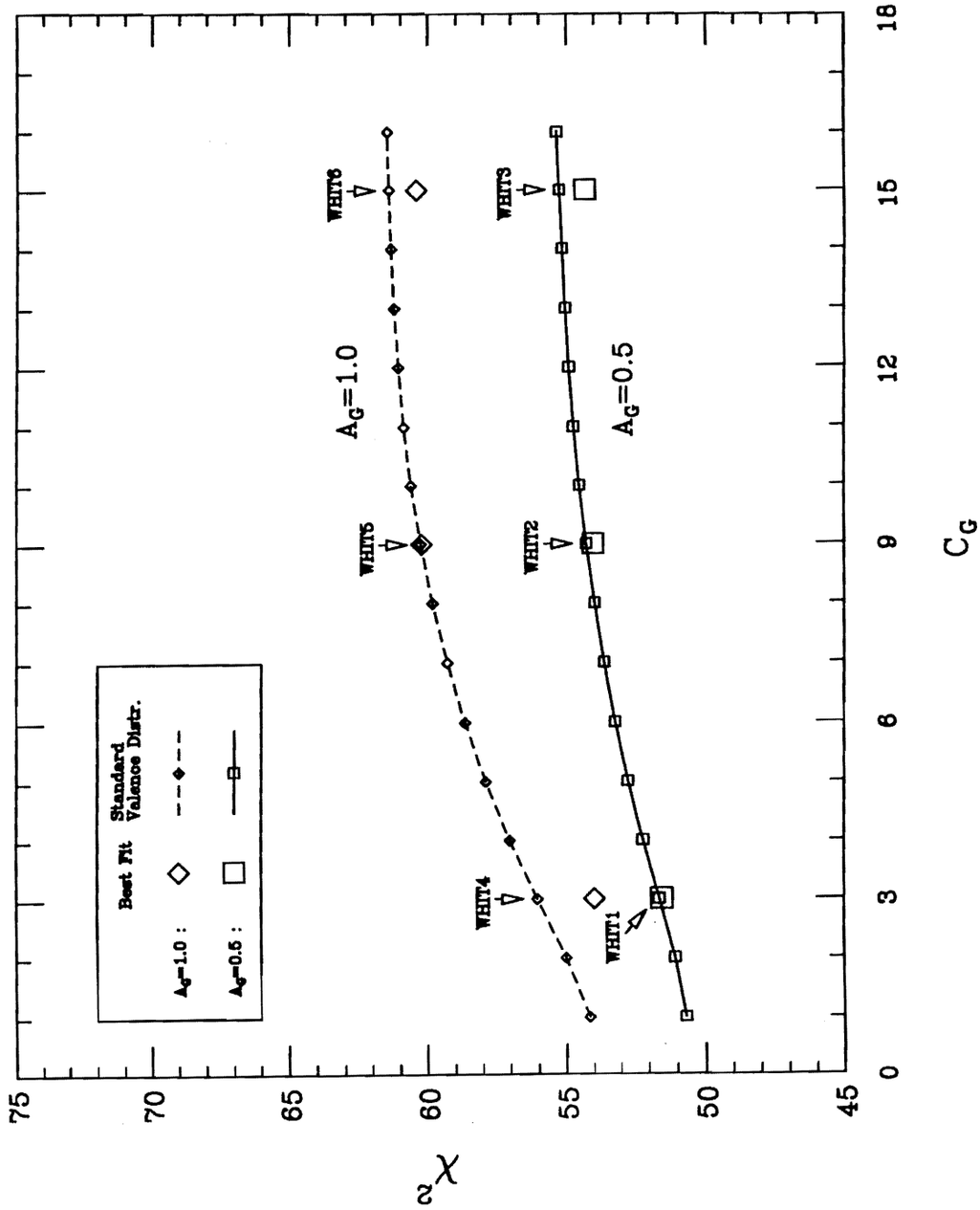
Best Fit
Standard Valence Distr.
A_G=1.0 :
A_G=0.5 :
A_G=1.0
A_G=0.5
WHIT1
WHIT2
WHIT3
WHIT4
WHIT5
WHIT6
χ^2
C_G
75
70
65
60
55
50
45
0
3
6
9
12
15
18

Fig. 3

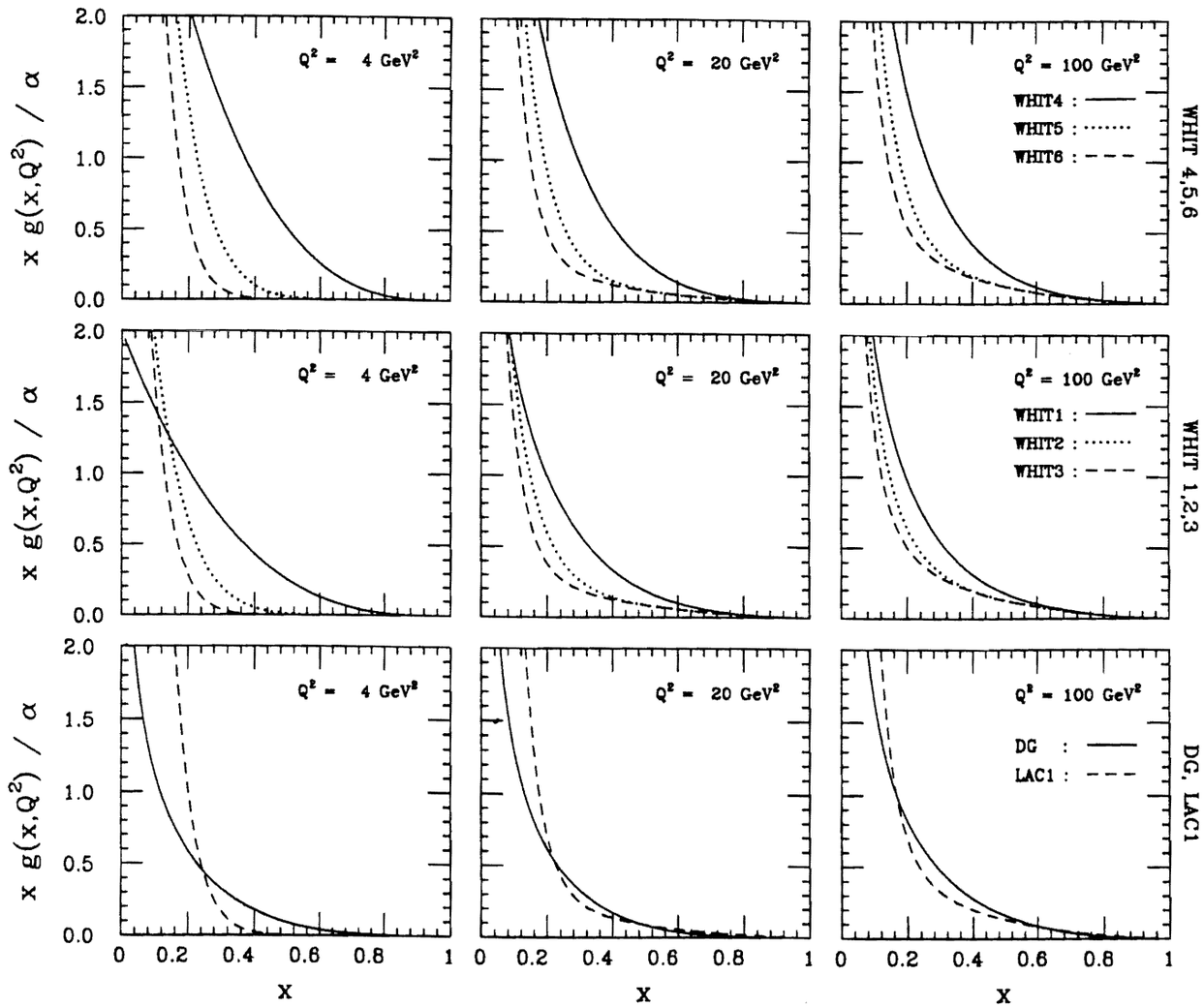
x g(x,Q²) / α
Q² = 4 GeV²
Q² = 20 GeV²
Q² = 100 GeV²
WHIT4 :
WHIT5 :
WHIT6 :
WHIT 4,5,6
WHIT1 :
WHIT2 :
WHIT3 :
WHIT 1,2,3
DG :
LAC1 :
DG, LAC1
x

Fig. 4

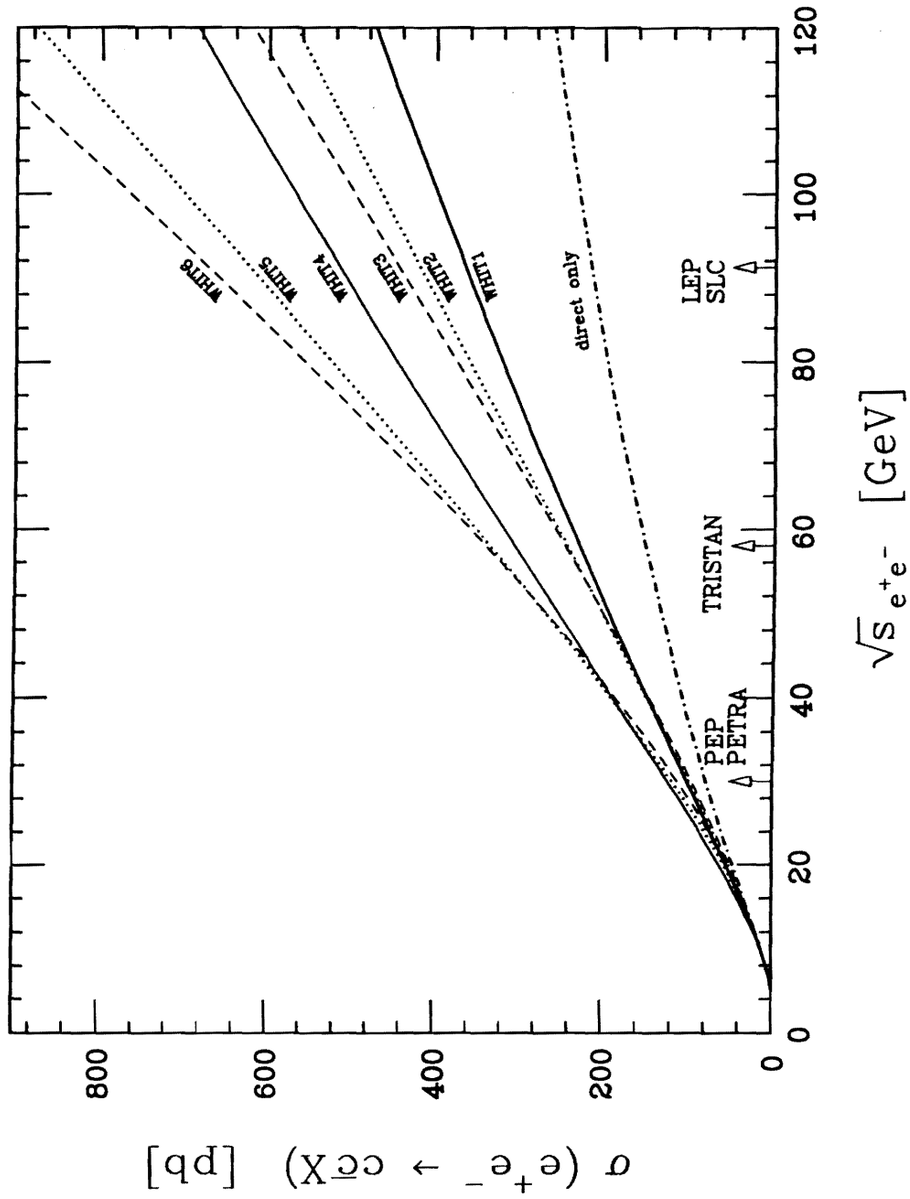
σ (e+e− → cc̄X) [pb]
0
200
400
600
800
0
20
40
60
80
100
120
√s e+e− [GeV]
PEP
PETRA
TRISTAN
LEP
SLC
direct only
WHIT1
WHIT2
WHIT3
WHIT4
WHIT5
WHIT6

Fig. 5